High Density of Quantum-Sized Silicon Nanowires with Different Polytypes Grown with Bimetallic Catalysts

Weixi Wang, Éric Ngo, Ileana Florea, Martin Foldyna, Pere Roca I Cabarrocas, Jean-Luc Maurice

ACS OMEGA

http://pubs.acs.org/journal/acsodf

Article

High Density of Quantum-Sized Silicon Nanowires with Different Polytypes Grown with Bimetallic Catalysts

Weixi Wang, Éric Ngo, Ileana Florea, Martin Foldyna, Pere Roca i Cabarrocas, and Jean-Luc Maurice*

Cite This: https://doi.org/10.1021/acsomega.1c03630

Read Online

ACCESS | Metrics & More | Article Recommendations | Supporting Information

ABSTRACT: When Si nanowires (NWs) have diameters below about 10 nm, their band gap increases as their diameter decreases; moreover, it can be direct if the material adopts the metastable diamond hexagonal structure. To prepare such wires, we have developed an original variant of the vapor−liquid−solid process based on the use of a bimetallic Cu−Sn catalyst in a plasma-enhanced chemical vapor deposition reactor, which allows us to prevent droplets from coalescing and favors the growth of a high density of NWs with a narrow diameter distribution. Controlling the deposited thickness of the catalyst materials at the sub-nanometer level allows us to get dense arrays (up to 6×10^{10} cm^{-2}) of very-small-diameter NWs of 6 nm on average (standard deviation of 1.6 nm) with crystalline cores of about 4 nm. The transmission electron microscopy analysis shows that both 3C and 2H polytypes are present, with the 2H hexagonal diamond structure appearing in 5−13% of the analyzed NWs per sample.

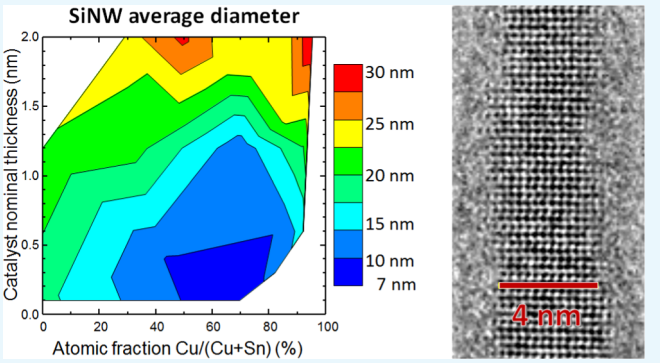

INTRODUCTION

Silicon nanowires (SiNWs) have garnered significant attention during the last decades due to their unique one-dimensional geometry, with properties suitable for different optoelectronic applications.[1−4] Early nanowire (NW) research focused on the control of their length, diameter, and density using different top-down and bottom-up approaches.[5,6] More recently, small-diameter NWs (below 10 nm) have been the subject of numerous studies due to the predicted quantum size effects.[1,7] In addition, it has been demonstrated that small-diameter NWs made of silicon can have the metastable hexagonal diamond crystalline structure—polytype 2H,[8] which radically changes their optoelectronic properties: in particular, very-small-diameter 2H NWs can have a direct band gap, which can be tuned by the diameter control.[7]

Small-diameter silicon quantum wires have been produced in the past either in negligible quantities (i.e., only a small fraction of the NWs had sufficiently small diameters) or via relatively complex approaches, often preventing the production of high densities of SiNWs.[9−16] The usual method to grow small-diameter NWs is the vapor−liquid−solid (VLS) process with gold as the catalyst. In this work, we have succeeded in growing very dense quantum wire arrays (up to 6×10^{10} cm^{-2}), using a variant of the VLS process based on the use of bimetallic Cu−Sn catalysts and plasma-enhanced chemical vapor deposition (PECVD) with SiH_4 gas.

The present work follows an observation of the metastable hexagonal diamond phase of Si (2H polytype) in NWs.[8] In that previous work, we had obtained SiNWs with the hexagonal structure using Sn as a catalyst and a Cu transmission electron microscopy (TEM) grid as a substrate.[8] However, the influence of Cu on the growth of 2H SiNWs was not considered at that time. As Cu can also be used as a catalyst for SiNW growth via the vapor−solid−solid (VSS) method at sufficiently high substrate temperatures,[17−19] its role was worth an investigation. Thus, in an effort to clarify the growth conditions that delivered this interesting structure,[7] we were led to develop SiNW growth using a catalyst made of Sn and Cu.

In this paper, we discuss the optimization of the Cu−Sn bimetallic catalyst to achieve very dense quantum wire arrays with an average diameter of around 6 nm; we also show that the density of 2H-polytype NWs depends on NW size but only little on the tested growth conditions. It remains relatively low, as we evidence the presence of the hexagonal diamond structure in the range of 5−13% of the analyzed NWs, depending on the experimental run. However, this translates in a very high density of about 3×10^9 cm^{-2}. Apart from the quantum size properties, such NWs could be beneficial for

Received: July 9, 2021
Accepted: September 20, 2021

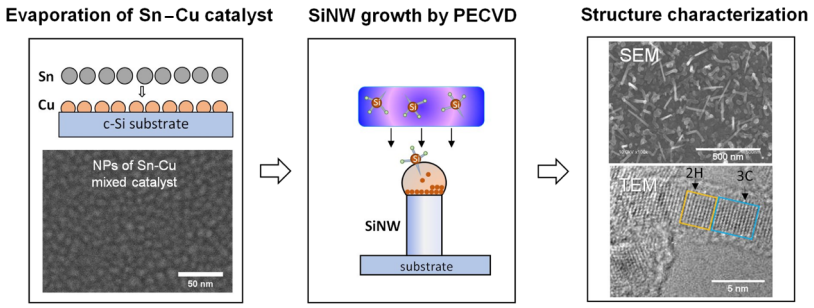

Figure 1. Schematic of the experiments reported. SiNWs were grown by PECVD with catalysts made of different amounts of Cu and Sn deposited sequentially (21 compositions in total, as shown in Figure 6; see Supporting Information, Table S1). The structure of the deposit, of the NWs, and of the catalysts was studied by SEM and TEM (see details in the Experimental Section).

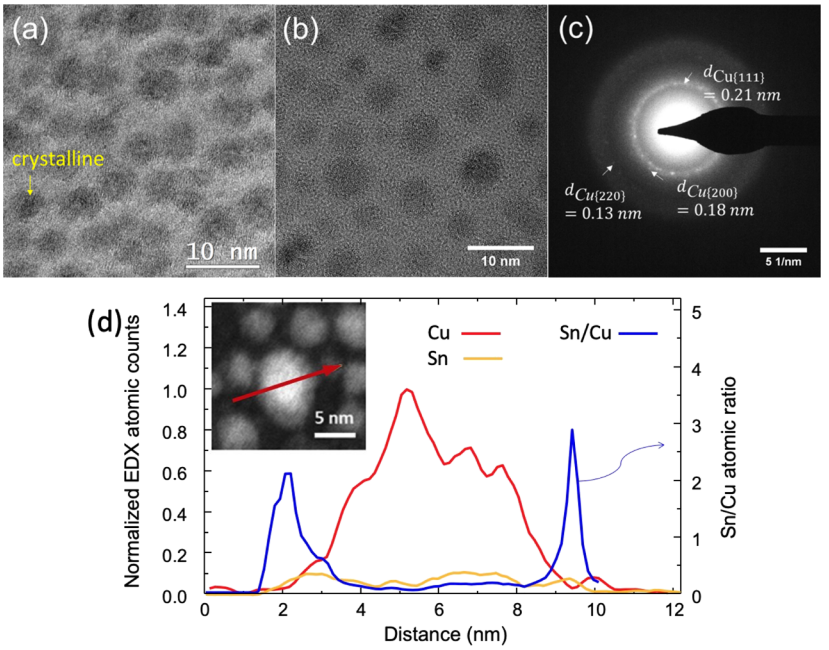

Figure 2. Mixed catalyst NPs of 0.6 nm Sn/0.6 nm Cu (70 at. % Cu) on the carbon membranes of TEM grids: (a) after annealing at 200 °C for 2 min in vacuum below 5×10^{-5} mbar in the PECVD reactor; (b) after the hydrogen plasma treatment at 200 °C. (c) Selected area diffraction pattern of the sample in (b) (150 nm diameter area). (d) EDX line scan on a NP of the same deposit after the hydrogen plasma treatment at 200 °C. High-angle annular dark field (HAADF) STEM image in inset. Normalized atomic counts along the red arrow for Cu (red) and Sn (brown-yellow) (left scale) and Sn/Cu atomic ratio (blue line, right scale).

applications requiring a high surface-to-volume ratio for catalysis, such as sensors or water splitting artificial leaves.[20−25]

Regarding the catalyst structure, we find that, in a broad range of composition, Cu−Sn NPs must be dual phased-liquid and solid - during SiNW growth, leading to a liquid-assisted VSS mechanism (LAVSS). This mechanism has been analyzed in detail in another paper.[26]

RESULTS AND DISCUSSION

Let us start by describing the logic underneath the experiments carried out in this work. The first important stage consisted in preliminary experiments—not described in this paper—of SiNW growth on Si with pure Sn as a catalyst. After having developed a reliable technique to transfer thin NWs to TEM grids for the TEM characterization of the structure, we observed the phase of tens of NWs to conclude that the use of pure Sn was producing no 2H structure. As this structure was present in NWs grown in the same runs on Cu TEM grids, another conclusion was that the element Cu was a mandatory catalyst component to obtain SiNWs with the hexagonal diamond structure. The question was then on the required concentration of Cu, which led us to the experiments described here. As will be seen in the following, this approach gave only a poor answer to the basic question of the 2H structure, but it allowed us to obtain interesting conclusions on the ability of Cu−Sn catalysts to deliver quantum-sized SiNWs.

Figure 1 summarizes the experiments we performed for this study: we varied the Cu/Sn ratio and Cu + Sn amount in the Cu−Sn catalysts prepared by sequential evaporation. Then, SiNWs were grown with the prepared catalysts in a PECVD reactor, first using the same standard conditions (see Supporting Information, Figure S1) to obtain the smallest NW diameter, then applying different conditions to try and increase the 2H ratio. Characterization was performed by scanning electron microscopy (SEM) and TEM. See details in the Experimental Section at the end of the paper.

In the following, we first investigate the structure of the Cu−Sn catalyst NPs systematically, as a function of composition and at the different stages of the process. For the sake of the chemical and crystallographic analyses, we use large NP sizes in

https://doi.org/10.1021/acsomega.1c03630
ACS Omega XXXX, XXX, XXX−XXX

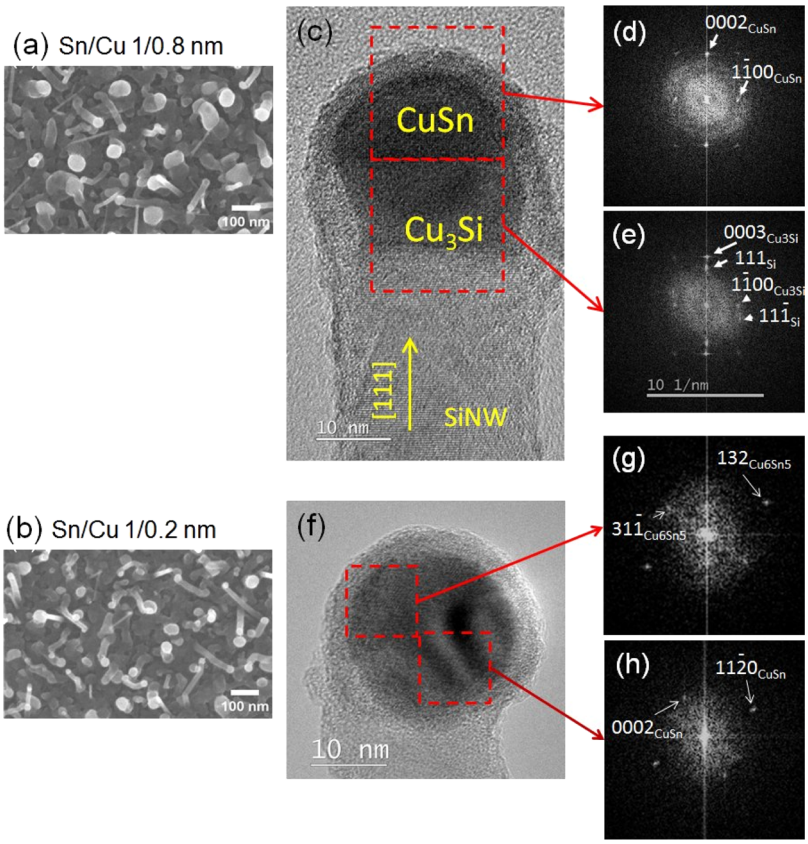

Figure 3. Comparison of SiNWs grown with majority Cu (a,c,d,e) and majority Sn (b,f,g,h) catalysts, with respective compositions: 1 nm Sn/0.8 nm Cu (65 at. % of Cu) and 1 nm Sn/0.2 nm Cu (31 at. % of Cu). (a,b) SEM images; (c) HRTEM image of a catalyst NP from the (majority Cu) sample of (a) and (d,e) FFTs of the squared areas in (c); and (f) HRTEM image of a catalyst NP from the (majority Sn) sample of (b) and (f,g) its FFTs. The SiNWs have been transferred from (100) c-Si substrates to TEM grids for their observation.

this part (up to 30 nm). We then study the influence of catalyst composition and deposited thickness on the value and distribution of NW diameters and finally discuss the occurrence of the metastable Si hexagonal-diamond phase in the thinnest wires.

Structure and Composition of Catalyst Nanoparticles. The bimetallic catalyst NPs are prepared by the sequential evaporation of Cu followed by Sn, at room temperature, simultaneously on (100) Si and a carbon-coated gold TEM grid (see the Experimental Section). Figure 2 shows the NPs obtained on the amorphous carbon (a-C) membrane of the TEM grid, with nominal deposited thicknesses of 0.6 nm Sn/0.6 nm Cu (70 at. % Cu). The as-deposited particles are mostly amorphous on the a-C substrate and remain mostly amorphous after annealing at 200 °C for 2 min in vacuum in the PECVD reactor (only one NP shows crystallographic planes as shown in Figure 2a). In contrast, the bimetallic catalyst NPs partially crystallize after the hydrogen plasma treatment at 200 °C (which is preliminary to the NW growth, see Supporting Information, Figure S1) (Figure 2b). A selected area electron diffraction pattern (Figure 2c) exhibits three diffraction rings corresponding to the (111), (200), and (220) planes of Cu (Figure 2c). That is, the NPs in Figure 2b contain Cu crystals, but there is no trace of crystalline Sn.

To determine the distribution of Sn in these mixed catalyst NPs after the hydrogen plasma treatment, we performed energy-dispersive X-ray (EDX) line scans in scanning TEM (STEM) mode. (We had to avoid EDX maps as the repeated scans destroyed the NPs.) The EDX line in Figure 2d goes through the center of a NP with a diameter of around 7 nm. The Cu signal (red line) has a much higher intensity than Sn (brown-yellow line) in the central brighter part; while in contrast, Sn dominates at the periphery, as shown by the blue line representing the Sn/Cu atomic ratio. Combining the abovementioned TEM results and EDX analysis of NPs after the hydrogen plasma treatment, we conclude that the NPs deposited on a-C consist of Cu nanocrystal cores covered by amorphous shells of a Sn-rich Sn−Cu alloy. Of course, surface tension equilibria are different on the present a-C substrate, compared to that on the crystalline silicon (c-Si) substrate. However, the TEM analyses carried out on the catalysts of NWs grown on c-Si (see below, Figures 3 and 4) suggest that the observed segregation between Cu and Sn is substrate-independent.

We have also analyzed the size and distribution of the particles at the substrate surface, as a function of catalyst-deposited thickness and composition. Figure S2 in Supporting Information presents the comparison between a deposit of 0.1 nm Sn/0.1 nm and that of 0.2 nm Sn/1 nm Cu. The diameter distribution increases with deposited thickness while keeping a significant amount of very small diameters.

To document the crystallographic and chemical properties of the catalyst after NW growth, we present in the following two catalyst compositions: (i) a majority Cu deposit, made of 1 nm Sn/0.8 nm Cu (65 at. % of Cu, Figure 3a) and (ii) a majority Sn deposit, made of 1 nm Sn/0.2 nm Cu (31 at. % of Cu, Figure 3b). We chose relatively large particles for the sake of clarity. The SiNWs are grown following a typical process at

https://doi.org/10.1021/acsomega.1c03630
ACS Omega XXXX, XXX, XXX−XXX

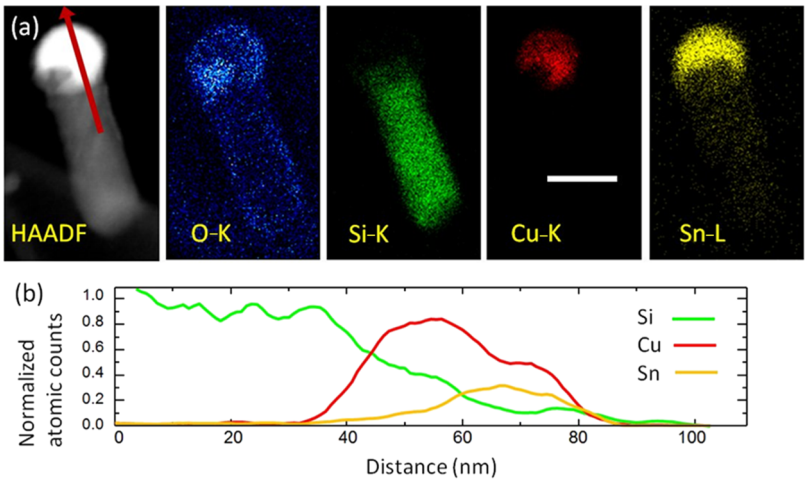

Figure 4. EDX mapping analysis of a SiNW synthesized with the majority Cu catalyst (1 nm Sn/0.8 nm Cu, 65 at. % Cu). (a) HAADF image and maps of the elements, scale bar = 50 nm; the contrasts of O−K and Sn−L images have been enhanced, compared to Si−K and Cu−K, for the sake of visibility. (b) Normalized atomic profiles of Si, Cu, and Sn along the red arrow in (a). Note the segregation between Sn and Cu in the catalyst.

416 °C (see Experimental Section and Supporting Information, Figure S1) on (100) Si and then transferred to gold TEM grids for TEM characterization. Figure 3c shows a high-resolution TEM (HRTEM) image of the top part of a SiNW grown with a majority Cu catalyst, in a projection close to the Si [1−10] zone axis. It is notable that the catalyst NP on top of the SiNW has a complex shape: there is a planar boundary separating the top of the NP (which has a darker contrast) from its bottom.

The top part of the NP has a hemispherical shape, including a dark amorphous-like contrast at the surface, while the bottom part exhibits crystalline facets, also covered by an amorphous-like matter, although with lighter contrast. In other words, the catalyst NP is mostly crystalline but the crystalline structure vanishes at the top of the particle, where we are tempted to attribute the amorphous layer to Sn that must have been liquid at the growth temperature. In contrast, the lighter amorphous structure around the base of the catalyst could come from an oxide.

When performing fast Fourier transforms (FFTs) of the HRTEM image in Figure 3c (squared areas), we find well-defined zone-axis patterns, very similar in either part of the catalyst (Figure 3d,e). Fitting the two patterns with JEMS[27] software, we find a good correspondence with the hexagonal CuSn structure,[28,29] an approximant of η-Cu_6Sn_5, in the [11−20] zone axis for the top part (Figure 3d) and with rhombohedral η Cu_3Si, also in the [11−20] zone axis in hexagonal coordinates[30] for the bottom part. (See Supporting Information for a detailed analysis.)

We thus conclude that the catalyst NP is essentially made, from top to bottom, of hexagonal Cu_6Sn_5 with, possibly, an amorphous Sn shell, and at the bottom, feeding the SiNW growth of a modified hexagonal cell of η-Cu_3Si. Quite remarkably, the three crystalline parts: (1) Cu_6Sn_5, (2) Cu_3Si, and (3) SiNW are epitaxially related: the two formers have their hexagonal base in common (see Figure S3), the Si NW has developed its (111) planes parallel to these bases, with ⟨112⟩ axes parallel to the hexagonal ⟨1−100⟩ axes of the catalyst. Considering the actual deformation of the present Cu_3Si cell, the in-plane mismatch between that cell and the cubic Si cell is of the order of 10%; it appears to be fully relaxed.

Figure 3f shows a HRTEM image of a SiNW synthesized with the majority Sn catalyst. In this case, the catalyst NP has a near-spherical shape and there is also, although less visible, a planar boundary separating the catalyst NP into two regions. However, we find no fit with a silicide in this case, the top and bottom parts having zone axes corresponding to Cu_6Sn_5 phases: the top part having the [5−78] zone axis of the monoclinic form of that compound (phase η', at equilibrium at room temperature)[31,32] and the bottom part having the [1−100] zone axis of the same CuSn cell as above (Cu_6Sn_5-η phase, at equilibrium between 189 and 408 °C).[32] At the growth temperature of 416 °C, that compound may have been present in a metastable state, or a higher Cu-concentration alloy (Cu_3Sn) may have existed. In any case, given the 69 at. % Sn, some of Sn (with dissolved Cu) must have remained outside the crystalline compounds during the growth, thus liquid at that time. The thick amorphous layer around the crystalline catalyst would be the remains of Sn that was in excess in the formation of the Cu−Sn alloy during cooling.

In order to confirm the position of Sn in catalyst NPs of the majority Cu deposit, presented in Figure 3c−e, we performed EDX mapping on a similar SiNW from the same deposit (Figure 4). Cu appears in most parts of the NP, whereas Sn is mostly detected in its top half part. We quantified the elemental composition of the whole NP area in the EDX map and obtained Cu and Sn with atomic fractions of 63.8 and 36.2%, respectively. It is very close to the nominal atomic ratio of the thermally evaporated materials (65 at. % of Cu and 35 at. % of Sn). This result shows that (i) the deposits remain uniform at the particle level—at least for this size of particle—and (ii) there is no catalyst leak during the NW growth. Considering the position of Sn in the particle and its very low amount in the bottom part, together with the presence of Si and Cu in the bottom part, it indeed supports the existence of a Cu silicide. Moreover, the fact that the Sn curve (brown-yellow, Figure 4b) has a higher intensity than either Cu or Si at the very top of the catalyst indicates that the amorphous structure at the top of the NP as shown in Figure 3c is indeed Sn-rich. The oxygen appearing in the catalyst (O−K image in Figure 4a) would come from a Si oxide that develops in the air after the NW growth.[33] We finally conclude that, after NW growth, the catalyst NPs obtained with 65 at. % of Cu in the

https://doi.org/10.1021/acsomega.1c03630
ACS Omega XXXX, XXX, XXX−XXX

deposit are essentially made of crystalline Cu_6Sn_5 and Cu_3Si, which would be solid at the growth temperature,[34,35] with a Sn-rich part, most probably liquid at the growth temperature (eutectic temperature of the Sn−Si system is 227 °C).[36]

Let us now summarize the differences between majority Cu and majority Sn catalyst compositions and extrapolate the crystallographic and compositional data deduced from Figures 3 and 4 (recorded at room temperature) to the growth temperature of 416 °C in view of the different phase diagrams.[31,32,34−37] The confrontation with the latter first shows that, in all cases except the very high Cu concentrations, there will be a liquid part in the catalysts during NW growth. Thus, these experiments indicate that SiNW growth using a Cu−Sn bimetallic catalyst is actually a LAVSS process. We have recently been able to confirm this using *in situ* TEM.[26] The majority Cu and majority Sn catalysts will differ by their solid content: (i) in the former, the solid part will be Cu_3Si during growth, while the excess Sn will be liquid, with Cu and Si in solution; (ii) in the latter in contrast, the solid part will be small as the solidus above the phases found is at 408 °C.[32] That solid part will preferentially be made of Cu_3Sn, metastable η-Cu_6Sn_5, or Cu_3Si, as we will discuss below.

We can now propose a mechanism for the catalyst formation and the catalyst evolution during the hydrogen plasma treatment and the NW growth (Figure 5). Let us recall that

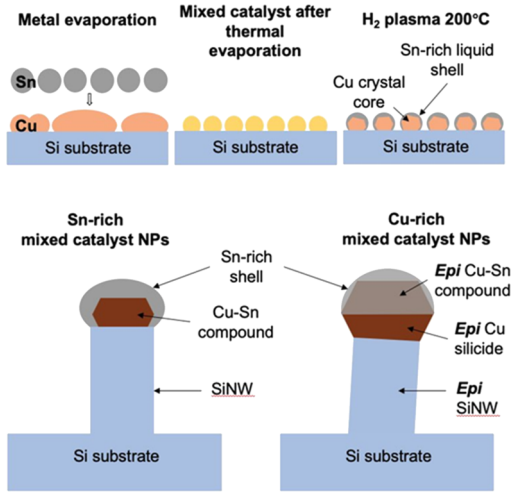

Figure 5. Schematic diagram of bimetallic Cu−Sn catalyst evolution at various stages of the SiNW growth process. The two figures at the bottom highlight the case of a NW growth led by a Sn-rich mixed catalyst NP (left) and a Cu-rich mixed catalyst NP (right).

Cu and Sn are evaporated sequentially, so that Sn covers Cu at the beginning. With the temperature increasing in the PECVD reactor, Cu would diffuse into Sn, rather than the opposite, as Cu has a high mobility and is the dominant diffusing species in the Cu−Sn system.[37] However, its solubility in Sn being low (0.018% at eutectic temperature[38]), it would not reach the concentration necessary for creating a new compound. After that, melting will occur when the substrate temperature reaches the melting temperature of the Cu−Sn eutectic (227 °C in the bulk probably below 200 °C in the present small NPs[39,40]). The rest of Cu would remain solid because bulk Cu has a high melting point of 1084.87 °C. After the hydrogen plasma treatment at 200 °C, Cu would crystallize and the Cu−Sn mixed catalyst NPs would consist of a Cu crystalline core and a Sn-rich, probably liquid, shell. When the temperature is increased to 416 °C for the NW growth, Cu-based compounds would form. When Si radicals from the plasma start introducing Si in the catalyst NPs, Cu−Si or Cu−Si−Sn compounds would develop, rather than a Si−Sn compound, as Si solubility in liquid Sn remains very low (<0.25%[36]). The balance between Cu_6Sn_5 and Cu_3Si evolves during growth and upon cooling.[26] Regarding Cu_3Si, the epitaxy of Si and the presence of Sn would stabilize a modified unit cell with a *c*-axis one-third of the normal *c*-axis of the (hexagonal) unit cell of rhombohedral η-Cu_3Si. The part of the catalyst NP where SiNW would develop would thus consist mostly of Cu_3Si. In the Sn-rich co-catalyst NPs, the Sn-rich shell would cover the crystalline core almost completely; Cu_3Si, in other respect, would completely disappear at the end of growth, having given back its Si atoms to the NW crystal. During the cooling process, after the NW growth, the molten Sn-rich alloy would solidify but keep the spherical shape. Sn finally appears as amorphous at room temperature.

Obtaining the Thinnest Nanowires. Let us now focus on the optimization of the Sn and Cu amounts to produce the smallest NW diameters, necessary to obtain quantum size effects and 2H hexagonal phase. We have explored SiNW growth with multiple combinations of evaporated Sn and Cu quantities (21 in total, see the Supporting Information), the PECVD conditions remaining the same. We have evidenced the presence of a deposited thickness threshold, below which the NW diameter distribution is narrow: see the discussion of this point in Supporting Information, Figures S4−S6. Figure 6 summarizes the influence of Cu and Sn deposited amounts on SiNW diameters. The SiNW average diameter D_{avg} has been measured from SEM images. We can see that, not surprisingly, it globally decreases as the catalyst total nominal thickness decreases. When the total nominal thickness of the two catalysts is larger than 1.2 nm, most samples have D_{avg} of around 20−30 nm. When the total nominal thickness is below 0.6 nm, most SiNW samples have D_{avg} smaller than 10 nm, except for the samples with either no Cu in them or almost no Sn (92 at. % of Cu). When the total nominal thickness of both catalysts is reduced to 0.2 nm (0.1 nm Sn/0.1 nm, 70 at. % of Cu), D_{avg} reaches the lowest values for the used PECVD growth conditions. By further reducing the catalyst thickness to 0.1 nm (0.05 nm Sn/0.05 nm Cu, 69.6 at. % of Cu), we do not decrease the SiNW diameters; instead, we only decrease NW density (see Supporting Information, Figure S7). As mentioned above, the diameter distribution also gets narrower with decreasing nominal thickness, with a lower sensitivity to the catalyst composition, see Supporting Information, Figure S6. Quite remarkably, the NW diameter depends on the total amount of catalyst as well as on the Cu/Sn ratio: the smallest diameters are obtained with compositions around 65 at. % of Cu, at a level of total catalyst amount, where pure Sn gives diameters thrice as large.

The epitaxial relationship that establishes itself in that case (Figure 3e) would be at the origin of a dominant ⟨111⟩ growth direction, which, in turn, would limit kinking and coalescence during the growth (see Supporting Information on this topic). The mixed catalyst composed of 0.1 nm Sn/0.1 nm Cu thus represents the optimized catalyst composition for the goal of quantum size SiNWs. Figure 7a,b show SiNWs grown with 0.1 nm Sn/0.1 nm Cu mixed catalyst using the typical PECVD conditions on (100) Si and carbon-coated gold TEM grid, respectively.

https://doi.org/10.1021/acsomega.1c03630
ACS Omega XXXX, XXX, XXX−XXX

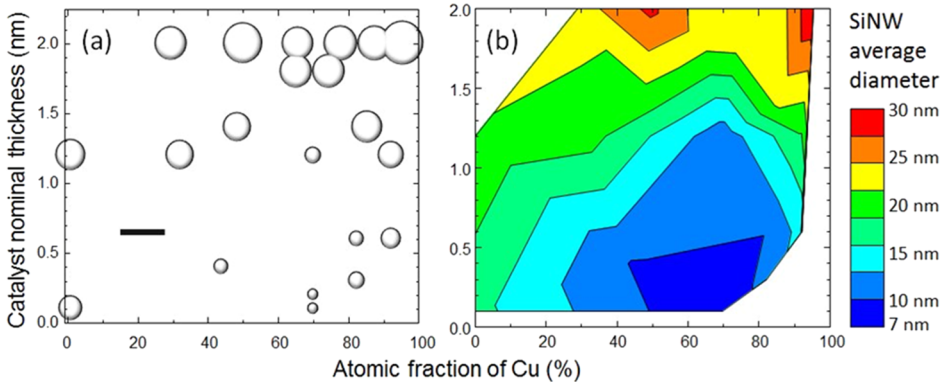

Figure 6. SiNW average diameter as a function of total nominal thickness (*Y* axis) and atomic fraction of Cu (*X* axis) in the multiphase catalyst. The SiNWs are grown on c-Si substrates and the average diameters of SiNWs are measured by SEM. (a) Plot showing the 21 data points; the size of the disks indicates the NW average diameter, scale bar = 30 nm. (b) Contour plot of the same data.

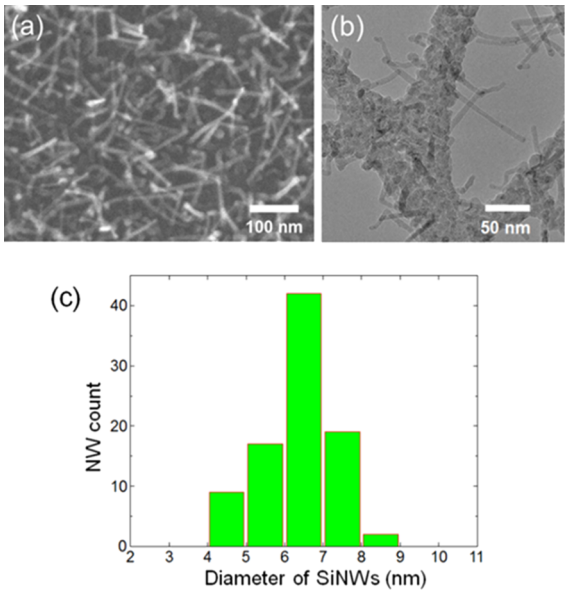

Figure 7. (a) SEM image of SiNWs synthesized with thermally evaporated films of nominal thicknesses of 0.1 nm Sn/0.1 nm Cu (70 at. % of Cu) on (100) Si substrate; (b) TEM image of the SiNWs grown under the same conditions on the carbon membrane of a gold TEM grid; and (c) histogram of SiNW diameter distribution measured from TEM images.

We have measured 100 SiNW diameters by TEM for this composition and plotted the result in Figure 7c. The SiNWs have a mean diameter of 6.3 nm with all values smaller than 9 nm. It is necessary to mention that the measured diameters include an amorphous oxide shell of around 1−2 nm, which was formed after the NW growth, leaving the crystalline core diameters of the SiNWs around 4 nm in average.

Thus, as shown in Figure 6 and illustrated in Figure 7, the NW diameter is quite sensitive to the Cu/Sn ratio. Let us now discuss the mechanism of this original property. The observation of the catalyst distribution before NW growth, as shown in Supporting Information, Figure S5, gives a clue: it shows that a deposit of Sn/Cu 1 nm/0.8 nm delivers smaller particles than thinner deposits of pure Sn (1 nm) or pure Cu (1 nm). We infer from this observation that solid Cu anchors Sn during deposition, which has the two effects of stopping the diffusion of Cu and stopping the coalescence of Sn droplets, thus drastically limiting the formation of larger catalysts and allowing for the growth of the smallest NWs. We were recently able to confirm this mechanism, thanks to *in situ* observations in TEM.[26] Thus, obtaining the smallest diameters needs the presence of a mixture of Cu and Sn. Why, then, ∼60% Cu? We show in Supporting Information (see Figure S4 and its discussion) that catalyst particles continue to coalesce after NWs have started to grow. Because of the much higher mobility of liquids, this mechanism must be more efficient for liquid catalysts than for solid catalysts. Thus, majority Sn catalysts, where the liquid part is larger (see above discussion), will tend to coalesce more during growth, delivering larger NWs. Then, why not pure Cu catalysts that are 100% solid, instead of the mixed solid Cu_3Si−liquid Sn catalysts? Let us mention at this stage that pure Cu catalysts did not provide SiNW growth at the growth temperature used; that metal is known to catalyze the CVD growth of SiNWs, with the VSS mechanism and under the form of solid Cu_3Si, but only above 500 °C.[18] At the lower temperature we used for the study of the catalyst composition as shown in Figure 6 (416 °C), however, catalysts with up to 95% Cu did work, delivering significantly larger NW diameters than the optimum concentration of 60−70% Cu. We attribute this effect to Sn acting as a diffusion barrier between the Cu NPs, as Sn is covering Cu (Figure 2), which would forbid Ostwald ripening of the particles during hydrogen plasma annealing.

If we now look at the NW density, it reaches a maximum of 6×10^{10} cm^{-2} for the deposit imaged in Figure 7a, where the average diameter is the smallest among all the samples we prepared to draw the map as shown in Figure 6b. The fact that this density maximum corresponds to the smallest NW diameter, although not surprising, is worth being noticed. It opens up the prospect of building NW carpets that would provide a well-defined NW diameter (see standard deviation in Figure S6b), which means a well-defined value of the band gap,[7] with a high enough density to deliver a usable absorption or emission of light.

Obtaining 2H Hexagonal Diamond Si Nanowires. In our previous work,[8] we had found SiNWs with the hexagonal 2H polytype. Moreover, since then, the hexagonal structure has been predicted to be stable in small-diameter SiNWs.[41] In the following, we thus analyze the NW structure and specifically focus on 2H polytype. In the sample shown in Figure 7b, we have analyzed 20 SiNWs in the [110]C/[1−210] zone axis, which is the only zone axis allowing to distinguish unambiguously the hexagonal structure from the twinned

https://doi.org/10.1021/acsomega.1c03630
ACS Omega XXXX, XXX, XXX−XXX

cubic structure.[8,42] Among them, there is one SiNW with a hexagonal phase (see Figure 8). That NW has a total diameter

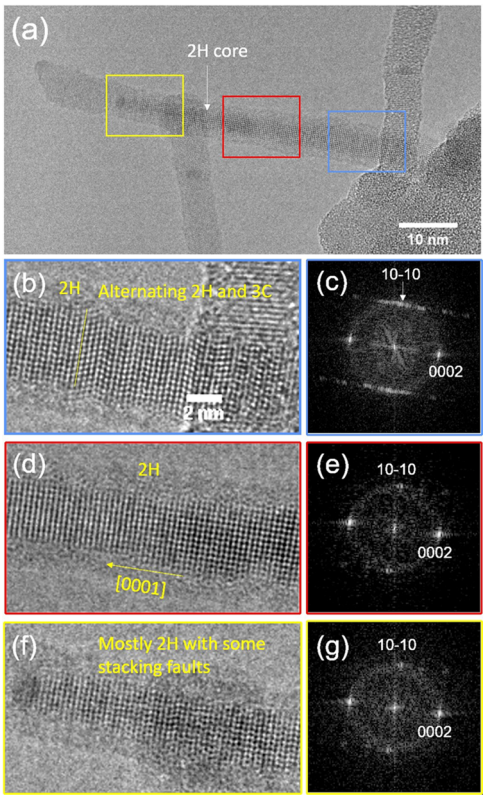

Figure 8. (a) HRTEM image of a SiNW with mostly the 2H phase; (b) alternating 2H and 3C domains at the bottom of the NW; (d) 2H phase in the middle; and (f) 2H phase with stacking faults at the top. The corresponding FFT images of (b,d,f) are shown in (c,e,g), respectively. Scale in (b) is for (b,d,f).

of 6.5 nm, with a crystalline core diameter of 4.2 nm. The NW has grown in the $\langle 0001\rangle_{2H}/\langle 111\rangle_{3C}$ axis: at the bottom (Figure 8b), it has alternating hexagonal and cubic domains, which is reflected in the FFT (Figure 8c). Then, it switches to a pure hexagonal phase in its middle part (Figure 8d). The FFT image in Figure 8e indicates that $d_{(0002)}$ = 0.314 nm and $d_{(10-10)}$ = 0.335 nm, with a $d_{(10-10)}/d_{(0002)}$ ratio of 1.068. The angle of (10−10) plane and (0002) plane is 90°. These values equal those of the theoretical 2H structure[43] within experimental error, which confirms that this SiNW has undoubtedly the 2H structure. At the top part of the crystalline core, the phase is mostly hexagonal with some stacking faults (Figure 8f,g). We have also performed SiNW growth at different substrate temperatures, with different silane partial pressures, and different catalysts on different substrates: we found hexagonal SiNWs for all conditions, with about the same recurrence. Table 1 summarizes the different conditions used in this work and their output in terms of SiNWs with the hexagonal phase, giving the 2H/3C ratio in TEM observations for each deposit. We have found that hexagonal Si can be obtained from 385 to 447 °C within the SiH_4 partial pressure range of 0.026−0.068 mbar on Cu TEM grid, carbon-coated gold TEM grid, and (100) Si wafer substrates. The SiNWs with the hexagonal phase have crystalline diameters ranging from 4.0 to 7.2 nm (see Supporting Information, Table S2 for the crystallographic data on these NW).

Thus, the 2H phase appears statistically in about 5−13% of SiNWs, depending on the sample, with no striking dependence on the tested process conditions. However, and quite remarkably, the hexagonal NWs always have very small diameters with the largest hexagonal SiNW found in this paper having a crystalline diameter of 7.2 nm. Only cubic phases were found in SiNWs with crystalline diameters larger than this value. This observation is consistent with the theoretical results predicting that the 2H phase would be favored in small NWs oriented in the [0001] direction.[41,44,45] To summarize, the present observations make it clear that having a small diameter is a necessary but not a sufficient condition for SiNWs to adopt the hexagonal 2H polytype, contrary to III−V semiconductor NWs, where this polytype is often found in large NWs.[46]

However, as in III−V semiconductor NWs, the phase chosen by the system is often not the equilibrium phase. In III−V materials, the hexagonal phase often occurs in large NWs for kinetic reasons,[47] while the cubic phase remains the equilibrium phase. In Si, the equilibrium phase in NWs with diameter below 13 nm should be the hexagonal phase, according to *ab initio* calculations;[41] here, we find that it is the case for only a small fraction of the wires of that size. Nevertheless, considering our SiNW density of 6×10^{10} cm^{-2} on (100) Si substrates, there should be about 3×10^9 SiNWs (5% fraction) with hexagonal phase per square centimeter, which is still a high density.

CONCLUSIONS

We have synthesized SiNWs using Cu−Sn bimetallic catalyst NPs. We conclude from post-growth TEM observations that, during SiNW growth, the mixed catalyst NPs are composed of a crystalline Cu-rich core and a liquid Sn-rich shell. For catalysts with a dominant Cu content, the liquid shell only covers a small area on top of what becomes a Cu_6Sn_5/Cu_3Si bi-crystal after cooling; while in the cases where Sn was dominant, the liquid shell would cover almost entirely a crystalline core made, after cooling, of Cu_6Sn_5. Therefore, we propose that the

Table 1. Catalyst Deposited Thickness, Growth Conditions, Diameter, and Proportion of 2H SiNWs in Six Growth Experiments

catalyst thickness Sn/Cu [nm/nm]	substrate	T [°C]	partial pressure of H_2/SiH_4 [mbar]	number 2H/3C SiNWs	crystalline diameter of 2H NWs [nm]
1/0	Cu grid	416	1.35/0.068	1/17	6.0
1/0	Cu grid	385	1.35/0.068	1/16	4.0
0.2/0.4	c-Si	416	1.35/0.068	2/15	4.4, 5.3
0.1/0.1	carbon membrane	416	1.35/0.068	1/19	4.2
0.1/0.1	c-Si	447	1.35/0.068	1/8	7.2
0.1/0.1	c-Si	416	2.55/0.026	1/16	5.7

https://doi.org/10.1021/acsomega.1c03630
ACS Omega XXXX, XXX, XXX−XXX

NW growth follows a LAVSS mechanism. This multiphase catalytic mechanism allowed us to obtain SiNW arrays with densities up to 6×10^{10} cm^{-2} with an average diameter of 6.3 nm and a diameter standard deviation of 1.6 nm. We attribute the ability to obtain very thin NWs with a narrow distribution to the fact that solid Cu would anchor the catalyst particles on the substrate and limit their coalescence before the growth. When considering the 1−2 nm thick amorphous shell that develops at the surface of NWs after the growth, such NWs have an average crystalline diameter below 5 nm. Such values have been obtained with an optimized mixed catalyst with nominal deposits of 0.1 nm Sn/0.1 nm Cu (70 at. % of Cu). SiNWs with the hexagonal phase have been observed within the crystalline diameter range of 4.0−7.2 nm; the yield of hexagonal SiNWs was found to be consistently around 5%, with up to 13% in a few samples. The hexagonal phase has been obtained in the temperature range from 385 to 447 °C and within the SiH_4 partial pressure range of 0.026−0.068 mbar, on both Cu TEM grid and (100) Si wafer substrates, using different catalyst compositions. Hexagonal Si appears statistically rarely and only in the small-diameter NWs.

Be they hexagonal or cubic, SiNWs with 4 nm as average crystalline diameter are in the size domain where the Si band gap depends on the NW diameter.[7] The ability to grow very dense and small-diameter SiNWs opens up the way to new applications, where carpets of semiconductor NWs would have their electronic and optical properties tuned by their average diameter.

EXPERIMENTAL SECTION

SiNWs were grown in a PECVD reactor with a bimetallic catalyst of Sn and Cu. Sn and Cu deposits were prepared using a BOC Edwards Auto 306 Evaporator FL 400. Cu was first evaporated on the substrates and then Sn was evaporated on top of Cu. Thus, the nominal thicknesses of the evaporated catalysts, measured by a quartz microbalance, could be controlled independently. Given the wetting of the metals on those substrates, NPs naturally form by atom aggregation upon thermal evaporation. For SiNW growth, we use (100) Si as the substrate. For the convenience of TEM observations of the as-deposited NPs in particular, a carbon-coated gold TEM grid is systematically placed in the evaporator beside the c-Si substrate. A gold grid is chosen instead of a Cu grid to allow EDX spectroscopy (EDX) analysis of Cu without the signal from the grid itself. The PECVD reactor operates at a radio frequency (RF) of 13.56 MHz to synthesize the SiNWs. The conditions for the PECVD process to synthesize SiNWs are the following. After the vacuum reaches 5×10^{-5} mbar, a hydrogen plasma treatment is carried out to remove the native oxide formed around the catalyst NPs during their transfer from the thermal evaporator to the PECVD reactor. During the treatment, the H_2 flow rate, the substrate temperature T, the gas pressure P, the RF plasma power density, and the duration time t are 100 sccm, 200 °C, 0.8 mbar, 56.7 mW cm^{-2}, and 2 min, respectively. Then, SiNWs are grown by adding a SiH_4 flow of 5 sccm and changing the process parameters to the following values: T of 416 °C, P of 1.42 mbar, and RF power density of 17 mW cm^{-2} for t = 3 min (see Supporting Information, Figure S1). This set of conditions is referred as the "typical PECVD conditions"; it has been used throughout the 21 deposits performed to make the NWs reported in Figure 6 (see a summary of the characteristics of the 21 deposits in the Supporting Information, Table S1). As explained in the text, other conditions have been investigated to try and improve the yield of 2H hexagonal Si. After the growth, SiNWs were observed by SEM using a Hitachi S-4800. The NW diameters were measured by SEM, unless otherwise specified. For each deposit, around 100 NWs were measured to provide a statistically relevant average diameter and a standard deviation (see Supporting Information, Figure S6). Then, some SiNWs were transferred from the c-Si substrate to TEM grids for high-resolution imaging and EDX analysis. The TEM equipment includes a JEOL 2010F (0.16 nm information limit) and a Thermo Fisher Titan 80-300 (0.12 nm information limit). The acceleration voltages utilized are 10 kV for SEM, 200 kV for the JEOL 2010F transmission electron microscope, and 300 kV for the Titan transmission electron microscope, respectively. EDX was performed with the Titan transmission electron microscope, which is equipped with an Oxford INCA system.

ASSOCIATED CONTENT

Supporting Information

The Supporting Information is available free of charge at https://pubs.acs.org/doi/10.1021/acsomega.1c03630.

Experimental process details and more characterizations, including statistical counting, SEM micrographs and discussion on the crystal phase of the catalyst (PDF)

AUTHOR INFORMATION

Corresponding Author

Jean-Luc Maurice − *École Polytechnique, LPICM, CNRS UMR 7647, Institut Polytechnique de Paris, 91120 Palaiseau, France;* orcid.org/0000-0002-5005-7174; Email: jean-luc.maurice@polytechnique.edu

Authors

Weixi Wang − *École Polytechnique, LPICM, CNRS UMR 7647, Institut Polytechnique de Paris, 91120 Palaiseau, France*

Éric Ngo − *École Polytechnique, LPICM, CNRS UMR 7647, Institut Polytechnique de Paris, 91120 Palaiseau, France;* Present Address: Now at Université Paris-Saclay, C2N, CNRS UMR 9001, 91120 Palaiseau, France

Ileana Florea − *École Polytechnique, LPICM, CNRS UMR 7647, Institut Polytechnique de Paris, 91120 Palaiseau, France;* orcid.org/0000-0002-2860-3992

Martin Foldyna − *École Polytechnique, LPICM, CNRS UMR 7647, Institut Polytechnique de Paris, 91120 Palaiseau, France;* orcid.org/0000-0001-8413-0504

Pere Roca i Cabarrocas − *École Polytechnique, LPICM, CNRS UMR 7647, Institut Polytechnique de Paris, 91120 Palaiseau, France;* orcid.org/0000-0003-2241-2762

Complete contact information is available at: https://pubs.acs.org/10.1021/acsomega.1c03630

Author Contributions

J.L.-M., M.F., and P.R.C. conceptualized the experiments. W.W. carried out the investigations, helped by M.F., I.F., and E.N.; W.W. analyzed the data; J.L.-M., P.R.C., and M.F. acquired the funding; J.L.-M. administrated the project; J.-L.M., M.F., and P.R.C. supervised the work; W.W. wrote the first draft of the paper, J.-L.M., M.F., and P.R.C. wrote the final version.

https://doi.org/10.1021/acsomega.1c03630
ACS Omega XXXX, XXX, XXX−XXX

Funding

This research was funded by the French National Research Agency, ANR, through the TEMPOS Equipex, pole Nano-MAX, grant number ANR-10-EQPX-50 and the HexaNW project, grant number ANR-17-CE09-0011.

Notes

The authors declare no competing financial interest.

■ ACKNOWLEDGMENTS

W.W. acknowledges the support from the Doctoral School of Institut Polytechnique de Paris. Thanks are due to the CIMEX—Centre Interdisciplinaire de Microscopie Electronique de l'X for the use of the electron microscopes at École Polytechnique.

■ ABBREVIATIONS

EDP, electron diffraction pattern; EDX, energy dispersive X-ray spectroscopy; FFT, fast Fourier transform; HAADF, high-angle annular dark field; HRTEM, high-resolution TEM; LAVSS, liquid-assisted VSS; NP, nanoparticle; NW, nanowire; PECVD, plasma-enhanced chemical vapor deposition; STEM, scanning TEM; TEM, transmission electron microscopy; VLS, vapor−liquid−solid; VSS, vapor−solid−solid

■ REFERENCES

(1) Hu, J.; Odom, T. W.; Lieber, C. M. Chemistry and Physics in One Dimension: Synthesis and Properties of Nanowires and Nanotubes. *Acc. Chem. Res.* **1999**, *32*, 435−445.
(2) Chung, S.-W.; Yu, J.-Y.; Heath, J. R. Silicon Nanowire Devices. *Appl. Phys. Lett.* **2000**, *76*, 2068−2070.
(3) Cui, Y.; Lieber, C. M. Functional Nanoscale Electronic Devices Assembled Using Silicon Nanowire Building Blocks. *Science* **2001**, *291*, 851−853.
(4) Schmidt, V.; Wittemann, J. V.; Senz, S.; Gösele, U. Silicon Nanowires: A Review on Aspects of Their Growth and Their Electrical Properties. *Adv. Mater.* **2009**, *21*, 2681−2702.
(5) Givargizov, E. I. Fundamental Aspects of Vls Growth. *J. Cryst. Growth* **1975**, *31*, 20−30.
(6) Misra, S.; Yu, L.; Chen, W.; Foldyna, M.; Roca i Cabarrocas, P. A Review on Plasma-Assisted Vls Synthesis of Silicon Nanowires and Radial Junction Solar Cells. *J. Phys. D: Appl. Phys.* **2014**, *47*, 393001.
(7) Amato, M.; Kaewmaraya, T.; Zobelli, A.; Palummo, M.; Rurali, R. Crystal Phase Effects in Si Nanowire Polytypes and Their Homojunctions. *Nano Lett.* **2016**, *16*, 5694−5700.
(8) Tang, J.; Maurice, J.-L.; Fossard, F.; Florea, I.; Chen, W.; Johnson, E. V.; Foldyna, M.; Yu, L.; Roca i Cabarrocas, P. Natural Occurrence of the Diamond Hexagonal Structure in Silicon Nanowires Grown by a Plasma-Assisted Vapour-Liquid-Solid Method. *Nanoscale* **2017**, *9*, 8113−8118.
(9) Chen, W.; Ahmed, H. Fabrication of high aspect ratio silicon pillars of. *Appl. Phys. Lett.* **1993**, *63*, 1116−1118.
(10) Holmes, J. D.; Johnston, K. P.; Doty, R. C.; Korgel, B. A. Control of Thickness and Orientation of Solution-Grown Silicon Nanowires. *Science* **2000**, *287*, 1471−1473.
(11) Cui, Y.; Lauhon, L. J.; Gudiksen, M. S.; Wang, J.; Lieber, C. M. Diameter-Controlled Synthesis of Single-Crystal Silicon Nanowires. *Appl. Phys. Lett.* **2001**, *78*, 2214−2216.
(12) Choi, Y.-K.; Zhu, J.; Grunes, J.; Bokor, J.; Somorjai, G. A. Fabrication of Sub-10-Nm Silicon Nanowire Arrays by Size Reduction Lithography. *J. Phys. Chem. B* **2003**, *107*, 3340−3343.
(13) Lu, X.; Hanrath, T.; Johnston, K. P.; Korgel, B. A. Growth of Single Crystal Silicon Nanowires in Supercritical Solution from Tethered Gold Particles on a Silicon Substrate. *Nano Lett.* **2003**, *3*, 93−99.
(14) Huang, Z.; Zhang, X.; Reiche, M.; Liu, L.; Lee, W.; Shimizu, T.; Senz, S.; Gösele, U. Extended Arrays of Vertically Aligned Sub-10 Nm Diameter [100] Si Nanowires by Metal-Assisted Chemical Etching. *Nano Lett.* **2008**, *8*, 3046−3051.
(15) Tan, Z.; Shi, W.; Guo, C.; Zhang, Q.; Yang, L.; Wu, X.; Cheng, G.-a.; Zheng, R. Fabrication of Ultra-Thin Silicon Nanowire Arrays Using Ion Beam Assisted Chemical Etching. *Nanoscale* **2015**, *7*, 17268−17273.
(16) Puglisi, R. A.; Bongiorno, C.; Caccamo, S.; Fazio, E.; Mannino, G.; Neri, F.; Scalese, S.; Spucches, D.; La Magna, A. Chemical Vapor Deposition Growth of Silicon Nanowires with Diameter Smaller Than 5 Nm. *ACS Omega* **2019**, *4*, 17967−17971.
(17) Yao, Y.; Fan, S. Si Nanowires Synthesized with Cu Catalyst. *Mater. Lett.* **2007**, *61*, 177−181.
(18) Arbiol, J.; Fontcuberta i Morral, A.; Estradé, S.; Peiró, F.; Kalache, B.; Roca i Cabarrocas, P.; Morante, J. R. Influence of the (111) Twinning on the Formation of Diamond Cubic/Diamond Hexagonal Heterostructures in Cu-Catalyzed Si Nanowires. *J. Appl. Phys.* **2008**, *104*, 064312.
(19) Kalache, B.; Cabarrocas, P. R. i.; Morral, A. F. i. Observation of Incubation Times in the Nucleation of Silicon Nanowires Obtained by the Vapor-Liquid-Solid Method. *Jpn. J. Appl. Phys.* **2006**, *45*, L190−L193.
(20) Peng, K.-Q.; Wang, X.; Lee, S.-T. Gas Sensing Properties of Single Crystalline Porous Silicon Nanowires. *Appl. Phys. Lett.* **2009**, *95*, 243112.
(21) Zhou, X. T.; Hu, J. Q.; Li, C. P.; Ma, D. D. D.; Lee, C. S.; Lee, S. T. Silicon Nanowires as Chemical Sensors. *Chem. Phys. Lett.* **2003**, *369*, 220−224.
(22) Zhang, R. Q.; Liu, X. M.; Wen, Z.; Jiang, Q. Prediction of Silicon Nanowires as Photocatalysts for Water Splitting: Band Structures Calculated Using Density Functional Theory. *J. Phys. Chem. C* **2011**, *115*, 3425−3428.
(23) Liu, C.; Tang, J.; Chen, H. M.; Liu, B.; Yang, P. A Fully Integrated Nanosystem of Semiconductor Nanowires for Direct Solar Water Splitting. *Nano Lett.* **2013**, *13*, 2989−2992.
(24) Liu, D.; Li, L.; Gao, Y.; Wang, C.; Jiang, J.; Xiong, Y. The Nature of Photocatalytic "Water Splitting" on Silicon Nanowires. *Angew. Chem., Int. Ed.* **2015**, *54*, 2980−2985.
(25) Peng, K.-Q.; Wang, X.; Li, L.; Hu, Y.; Lee, S.-T. Silicon Nanowires for Advanced Energy Conversion and Storage. *Nano Today* **2013**, *8*, 75−97.
(26) Ngo, É.; Wang, W.; Bulkin, P.; Florea, I.; Foldyna, M.; Roca i Cabarrocas, P.; Maurice, J.-L. Liquid-Assisted Vapor−Solid−Solid Silicon Nanowire Growth Mechanism Revealed by in Situ Tem When Using Cu−Sn Bimetallic Catalysts. *J. Phys. Chem. C* **2021**, *125*, 19773.
(27) Stadelmann, P. Jems-Swiss. https://www.jems-swiss.ch/ (accessed on September 6, 2021).
(28) Bernal, J. D. The Complex Structure of the Copper-Tin Intermetallic Compounds. *Nature* **1928**, *122*, 54.
(29) Wyckoff, R. W. G. *Crystal Structures*, 2nd ed.; Interscience Publishers: New York, New York, 1963; Vol. *1*, pp 85−237.
(30) Wen, C.-Y.; Spaepen, F. In situ electron microscopy of the phases of Cu_3Si. *Philos. Mag.* **2007**, *87*, 5581−5599.
(31) Larsson, A.-K.; Stenberg, L.; Lidin, S. The superstructure of domain-twinned η'-Cu_6Sn_5. *Acta Crystallogr., Sect. B: Struct. Sci.* **1994**, *50*, 636−643.
(32) Fürtauer, S.; Li, D.; Cupid, D.; Flandorfer, H. The Cu-Sn phase diagram, Part I: New experimental results. *Intermetallics* **2013**, *34*, 142−147.
(33) Wang, W.; Ngo, É.; Florea, I.; Foldyna, M.; Roca i Cabarrocas, P.; Maurice, J.-L. Room Temperature Growth of Silica Nanowires Synthesized with Sn-Cu Bimetallic Seeds, *Phys. Stat. Sol. A*, 2021, DOI: 10.1002/pssa.202100409.
(34) Song, Y.; Su, X.; Liu, Y.; Peng, H.; Wu, C.; Wang, J. Phase Equilibria of the Cu-Si-Sn System at 700 and 500 °C. *J. Phase Equilib. Diffus.* **2015**, *36*, 493−502.
(35) Olesinski, R. W.; Abbaschian, G. J. The Cu−Si (Copper-Silicon) system. *Bull. Alloy Phase Diagrams* **1986**, *7*, 170−178.
(36) Olesinski, R. W.; Abbaschian, G. J. The Si−Sn (Silicon−Tin) system. *Bull. Alloy Phase Diagrams* **1984**, *5*, 273−276.

https://doi.org/10.1021/acsomega.1c03630
ACS Omega XXXX, XXX, XXX−XXX

(37) Tu, K.-N. Copper−Tin Reactions in Bulk Samples. In *Solder Joint Technology: Materials, Properties, and Reliability*; Springer: New York, 2007; pp 37−71.
(38) Snugovsky, L.; Cermignani, C.; Perovic, D. D.; Rutter, J. W. The Solid Solubility of Ag and Cu in the Sn Phase of Eutectic and near-Eutectic Sn-Ag-Cu Solder Alloys. *J. Electron. Mater.* **2004**, *33*, 1313−1315.
(39) Cui, Q.; Gao, F.; Mukherjee, S.; Gu, Z. Joining and Interconnect Formation of Nanowires and Carbon Nanotubes for Nanoelectronics and Nanosystems. *Small* **2009**, *5*, 1246−1257.
(40) Jeong, S.; Woo, K.; Kim, D.; Lim, S.; Kim, J. S.; Shin, H.; Xia, Y.; Moon, J. Controlling the Thickness of the Surface Oxide Layer on Cu Nanoparticles for the Fabrication of Conductive Structures by Ink-Jet Printing. *Adv. Funct. Mater.* **2008**, *18*, 679−686.
(41) Béjaud, R.; Hardouin Duparc, O. Stabilizing the Hexagonal Diamond Metastable Phase in Silicon Nanowires. *Comput. Mater. Sci.* **2021**, *188*, 110180.
(42) den Hertog, M. I.; Cayron, C.; Gentile, P.; Dhalluin, F.; Oehler, F.; Baron, T.; Rouviere, J. L. Hidden Defects in Silicon Nanowires. *Nanotechnology* **2012**, *23*, 025701.
(43) Rödl, C.; Sander, T.; Bechstedt, F.; Vidal, J.; Olsson, P.; Laribi, S.; Guillemoles, J. F. Wurtzite Silicon as a Potential Absorber in Photovoltaics: Tailoring the Optical Absorption by Applying Strain. *Phys. Rev. B: Condens. Matter Mater. Phys.* **2015**, *92*, 045207.
(44) Akiyama, T.; Nakamura, K.; Ito, T. Stacking Sequence Preference of Pristine and Hydrogen-Terminated Si Nanowires on Si(111) Substrates. *Phys. Rev. B: Condens. Matter Mater. Phys.* **2006**, *74*, 033307.
(45) Kagimura, R.; Nunes, R. W.; Chacham, H. Structures of Si and Ge Nanowires in the Subnanometer Range. *Phys. Rev. Lett.* **2005**, *95*, 115502.
(46) Harmand, J.-C.; Patriarche, G.; Glas, F.; Panciera, F.; Florea, I.; Maurice, J.-L.; Travers, L.; Ollivier, Y. Atomic Step Flow on a Nanofacet. *Phys. Rev. Lett.* **2018**, *121*, 166101.
(47) Glas, F.; Harmand, J.-C.; Patriarche, G. Why Does Wurtzite Form in Nanowires of III-V Zinc Blende Semiconductors? *Phys. Rev. Lett.* **2007**, *99*, 146101.

https://doi.org/10.1021/acsomega.1c03630
ACS Omega XXXX, XXX, XXX−XXX